ChemComm

COMMUNICATION

View Article Online
View Journal | View Issue

Cite this: *Chem. Commun.*, 2020, **56**, 9858

Received 10th June 2020,
Accepted 16th July 2020

DOI: 10.1039/d0cc04054a

rsc.li/chemcomm

Precise tetrafunctional streptavidin bioconjugates towards multifaceted drug delivery systems†

Dongdong Xu,[a] Astrid Johanna Heck,[a] Seah Ling Kuan,[ab] Tanja Weil[ab] and Seraphine V. Wegner*[ac]

The preparation of precise macromolecules with multiple functionalities remains a challenge in drug delivery. Here, a method to prepare stoichiometrically precise tetrafunctional streptavidin conjugates is presented with an exemplary structure combining exactly one fluorescent label, one cell targeting group, one nucleus penetrating peptide and one drug molecule.

In drug delivery, the availability of macromolecules combining several different functionalities is often crucial to impart bioactivity, traceability and labelling. Beside the cytotoxicity of a drug designed as an anti-cancer agent, its targeted delivery to the right cell type and intracellular location as well as the real-time monitoring of the therapeutic are all desired features to increase the efficacy and safety.[1] Yet, combining multiple functional groups in a single macromolecule is non-trivial.[2–6] Multifunctionalization has mostly been realized with nanocarriers[7] that are large enough to harbor many molecules but with limited control of the number of functional groups that are incorporated. These have been decorated with targeting ligands like antibodies[8] or peptides[9] and loaded with known small molecule drugs and imaging probes.[10,11] Macromolecular drugs with many functionalities are far less common, due to the challenges in synthesis, solubility and preserving the activity. Even more important, general methods for the straightforward optimization of multifunctional molecules that would allow for efficient design and screening are missing.

Multivalent protein assemblies, which provide the advantages of simple production, monodisperse size and structure,[12] have been developed for specific targeting and delivery. In particular, streptavidin with its four independent biotin binding pockets, extraordinarily high affinity (K_d = 10^{-14}) and low exchange rates is an attractive scaffold.[13] Moreover, the mature biotin labelling technology provides a large repertoire of biotinylated molecules with targeting, sensing, diagnostic and therapeutic entities. Yet, it is still challenging to produce structurally defined streptavidin conjugates with more than one type of biotin labeled molecule and precise stoichiometry. More precisely, when four different biotinylated molecules are mixed with streptavidin, a statistical mixture forms where only 1 of the 35 possible products is the desired tetrafunctional one. It is challenging if not impossible to separate the desired product, which contains all four functional labels from the mixture of defective structures and would result in extremely low yield. So far, only precise streptavidin conjugates with four different single stranded DNA have been prepared, which limits the type of functional groups in the macromolecular assembly.[6] Other approaches to deal with multivalency or desymmetrization of streptavidin include the development of monovalent streptavidin to specifically label one receptor at the cell surface without artificially inducing clustering[14] and to use solid support-based assemblies to sterically block some of the biotin binding sites.[15] Nevertheless, incorporating more than two functional entities without restriction on one streptavidin in a controlled way is still elusive.

Herein, we describe a general method to prepare stoichiometrically exact tetrafunctional streptavidin conjugates offering great flexibility in conjugated molecules (Fig. 1A). For example, we combined a fluorescent label (atto-565-biotin), a cell type specific targeting group (folic acid–biotin), a nuclear localization peptide (nucleus penetrating peptide–biotin)[16] and an *anti*-cancer drug (doxorubicin–biotin) within one bioconjugate, which allowed for specific and efficient cellular toxicity towards cancer cells and its simultaneous detection.

The assembly of precise tetrafunctional streptavidin conjugates relies on a peptide with an iminobiotin and 12 histidines, named the Ibio-His-tag (Fig. 1B). The Ibio-His-tag allows separating streptavidin (S) conjugates with different numbers of bound Ibio-His-tags on a Cu^{2+}-NTA column using an imidazole elution gradient (S(Ibio-His-tag)$_{1–4}$).[17] Secondly, the pH-dependent binding of iminobiotin to streptavidin[18] allows releasing the Ibio-His-tag from the conjugates by lowering the pH to 3.5 and linking a biotinylated molecules with precise stoichiometry. Previous reports have shown the preparation of monofunctional streptavidin conjugates with precise stoichiometries and different vacancies using this method.[19]

[a] *Max Planck Institute for Polymer Research, Ackermannweg 10, 55128 Mainz, Germany*
[b] *Institute of Inorganic Chemistry I, Ulm University, Albert-Einstein-Allee 11, 89081 Ulm, Germany*
[c] *Institute of Physiological Chemistry and Pathobiochemistry, University of Münster, Waldeyerstr. 15, 48149 Münster, Germany. E-mail: wegnerse@exchange.wwu.de*

† Electronic supplementary information (ESI) available. See DOI: 10.1039/d0cc04054a

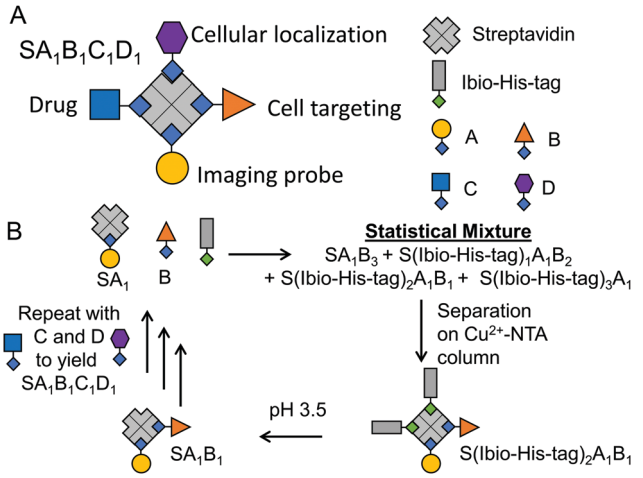

Fig. 1 Strategy for preparing tetrafunctional streptavidin–biotin conjugates. (A) Four different biotinylated molecules for therapeutic activity, cell targeting, intracellular localization and theranostics are combined into one streptavidin conjugate. (B) Each of the functionalities is added one by one going through cycles of forming statistical mixtures of products containing different numbers of Ibio-His-tags, which are separated on a Cu^{2+}-NTA column. The biotin binding pockets made accessible again at lower pH, allowing the repetition of the synthesis and purification cycles.

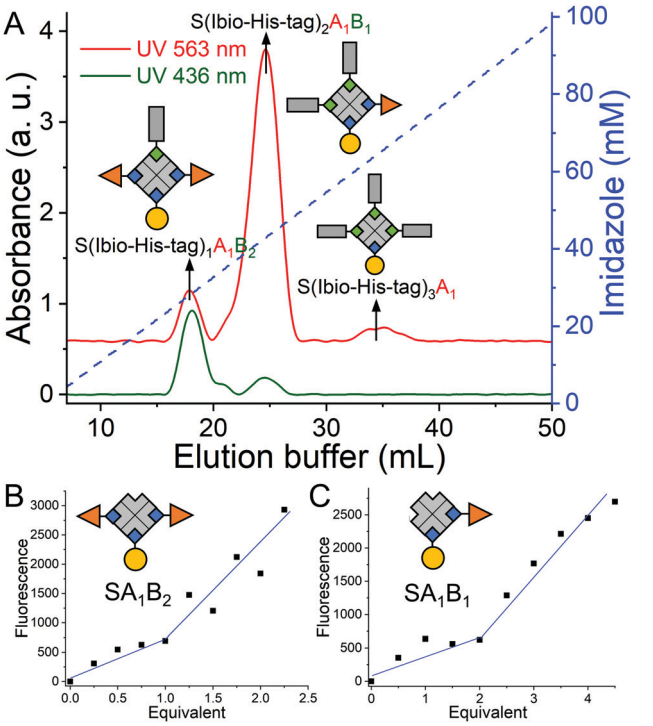

Fig. 2 Preparation and characterization of difunctional streptavidin conjugates. (A) Chromatogram of the reaction mixture of SA_1, atto-425-biotin and Ibio-His-tag. 1st peak: $S(Ibio\text{-}His\text{-}tag)_1A_1B_2$ (27.8 mM imidazole, area 9.7%), 2nd peak: $S(Ibio\text{-}His\text{-}tag)_2A_1B_1$ (43.6 mM imidazole, area 85.2%), 3rd peak: $S(Ibio\text{-}His\text{-}tag)_3A_1$ (63.2 mM imidazole, area 5.1%). SA_1B_3 (Area 2.5%) washed off without imidazole. The accessible biotin binding pockets of the species in the (B) 1st and (C) 2nd peak were titrated with biotin-5-fluorescein, A: atto-565-biotin, B: atto-425-biotin.

Repeating this chemistry over multiple cycles, we assemble in a step by step fashion up to four biotinylated molecules; in this case various fluorophores, on a single streptavidin with exact control over the stoichiometry ($SA_1B_1C_1D_1$, A: atto-565-biotin, B: atto-425-biotin, C: atto-665-biotin, D: biotin-5-fluorescein) (Fig. 1). To introduce the second biotinylated molecule, we started with a mono atto-565 labeled streptavidin, SA_1, with three available biotin binding pockets, which was prepared as described previously.[19] When SA_1 (1 μM) was incubated with a second biotinylated molecule, atto-425-biotin (B, 2 μM) and the Ibio-His-tag (2 μM), a statistical mixture composed of SA_1B_3, $S(Ibio\text{-}His\text{-}tag)_1A_1B_2$, $S(Ibio\text{-}His\text{-}tag)_2A_1B_1$ and $S(Ibio\text{-}His\text{-}tag)_3A_1$ formed. Subsequently, the mixture separated on a Cu^{2+}-NTA agarose column, where conjugate without the tag, SA_1B_3, was washed off and species bearing higher numbers of tag eluted at higher imidazole concentrations. In the chromatogram, three peaks with an absorbance typical for atto-565 (A) at 563 nm were observed, but only the first two absorbed at 436 nm typical for atto-425 (B) (Fig. 2A). Thus, the peaks with increasing imidazole concentration were assigned as $S(Ibio\text{-}His\text{-}tag)_1A_1B_2$, $S(Ibio\text{-}His\text{-}tag)_2A_1B_1$ and $S(Ibio\text{-}His\text{-}tag)_3A_1$, respectively.

To confirm the identity of the species, first the Ibio-His-tag was removed at lowered pH to yield well defined difunctionalized streptavidin conjugates with available biotin binding pockets, SA_1B_2 and SA_1B_1. Subsequently, the number of accessible biotin binding pockets was determined through the titration with biotin-5-fluorescein, which is quenched upon binding to streptavidin (Fig. 2B and C).[20] The streptavidin conjugates in the first (SA_1B_2) and second (SA_1B_1) peak reacted with one and two equivalents of biotin-5-fluorescein, respectively.

The third biotinylated molecule was added onto the SA_1B_1 bioconjugate repeating the same protocol. Shortly, SA_1B_1 (A: atto-565-biotin, B: atto-425-biotin, 1 μM) was incubated with atto-665-biotin (C, 1.5 μM) and Ibio-His-tag (1.5 μM) and the reaction products were separated on a Cu^{2+}-NTA agarose column. While the specie without the biotin tag, $SA_1B_1C_2$, did not bind to the column, two species eluted at different imidazole concentrations (Fig. 3A). The first peak was assigned as $S(Ibio\text{-}His\text{-}tag)_1A_1B_1C_1$ because it only has one Ibio-His-tag and was the only species to absorb at 663 nm typical for atto-665 (C). The second peak at higher imidazole concentrations, was identified as $S(Ibio\text{-}His\text{-}tag)_2A_1B_1$ since it has two tags.

Finally, to form an exact tetrafunctional streptavidin conjugate, $SA_1B_1C_1D_1$, it is sufficient to remove the Ibio-His-tag from $S(Ibio\text{-}His\text{-}tag)_1A_1B_1C_1$ at lowered pH and add one equivalent of the desired biotinylated molecule. When the above prepared $SA_1B_1C_1$ was titrated with biotin-5-fluorescein (D), it reacted with one equivalent yielding $SA_1B_1C_1D_1$ (Fig. 3B). This experiment also confirms the structure of the $SA_1B_1C_1$ conjugate with one open biotin binding pocket.

The importance of forming precise multifunctional streptavidins and not statistical mixtures was already apparent from the Förster resonance energy transfer (FRET) in $SA_1B_1C_1$ (A: atto-565-biotin, B: atto-425-biotin, C: atto-665-biotin). When we excited the atto-425 at 400 nm, there were three emission peaks at 476, 594 and 690 nm for atto-425, atto-565 and atto-665, respectively due to their close proximity (Fig. 3C, Fig. S1, ESI†). On the other hand, when we formed a statistical mixture of conjugates by mixing one equivalent of each of the three fluorophores with streptavidin, there was only one peak at 476 nm upon excitation at 400 nm. Moreover, the characteristic UV-Vis absorbance peaks of the three fluorophores in

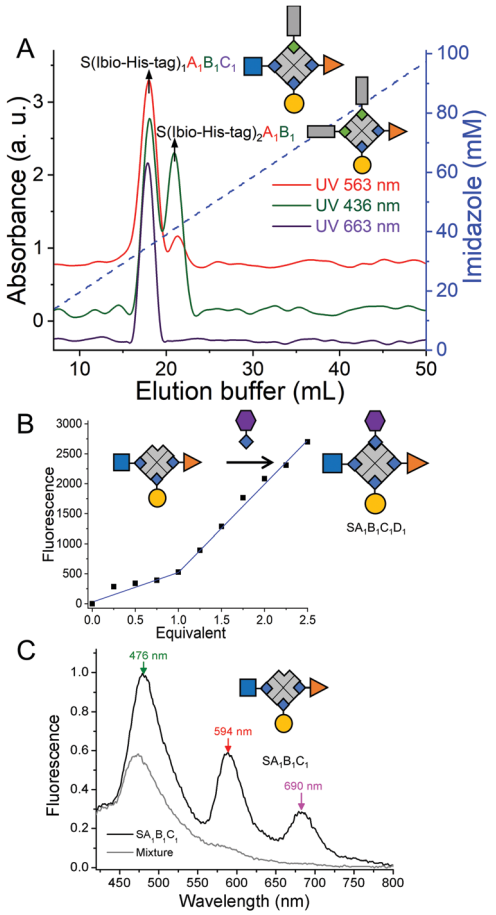

Fig. 3 Preparation and characterization of tri- and tetra-functional streptavidin conjugates. (A) Chromatogram of the reaction mixture of SA_1B_1, atto-665-biotin and Ibio-His-tag. 1st peak: S(Ibio-His-tag)$_1$$A_1B_1C_1$ (34.1 mM imidazole, area 84.5%), 2nd peak: S(Ibio-His-tag)$_2$$A_1B_1$ (41.5 mM imidazole, area 16.5%). $SA_1B_1C_2$ (area 2.3%) washed off without imidazole. (B) $SA_1B_1C_1$ required one equivalent of the biotin-5-fluorescein in the titration to saturate the biotin binding site, forming the tetrafunctional streptavidin conjugate, $SA_1B_1C_1D_1$. (C) Fluorescence emission spectrum (λ_{Ex} = 400 nm) of the precise $SA_1B_1C_1$ and a statistical mixture of streptavidin conjugates (S mixed with 1 equivalent of A, B and C). A: atto-565-biotin, B: atto-425-biotin, C: atto-665-biotin, D: biotin-5-fluorescein.

$SA_1B_1C_1$ support the stoichiometry of the complex (A : B : C = 1.0 : 1.2 : 1.0) (Fig. S2, ESI†).

Next, we set out to combine four functionalities in one streptavidin conjugate to underline the potential for designing optimized cancer theranostics. For this purpose, we integrated the following functionalities within a single macromolecule: (i) atto-565-biotin (A) as a fluorescent label for tracking the fate of the conjugates, (ii) folic acid–PEG–biotin (F) for selective targeting of folic acid receptor positive cancer cells such triple negative breast cancer cells (MDA-MB-231),[21] (iii) doxorubicin–biotin (D) (Fig. S3–S5, ESI†) as a broadly applied *anti*-cancer drug and (iv) a nucleus penetrating peptide–biotin (C) (Fig. S6 and S7, ESI†) for the targeted delivery of doxorubicin to the relevant subcellular compartment.[22] Each of these biotinylated molecules was added sequentially according to the above order following the same method as described above (Fig. S8 and S9, ESI†). The yield of each step depends on the biotinylated molecules and was not the same as for the previous tetrafunctional conjugate.

Each of the biotinylated molecules within the tetrafunctional streptavidin conjugate should contribute to the overall function.

The folic acid in the conjugate is supposed to increase the selectivity for cancer cell types, which are folate receptor positive. To demonstrate this point, the uptake of streptavidin conjugates with (SA_1F_1, SA_1F_2 and SA_1F_3) and without folic acid (SA_1) was evaluated in the folate receptor positive breast cancer cells, MDA-MB-231, and folate receptor-negative MCF-7 cells. After 4 h incubation the fluorescence signal from the atto-565 (A) showed that MDA-MB-231 cells incubated with different SAF conjugates were much brighter than MCF-7 cells (Fig. 4A and Fig. S10–S12, ESI†). Moreover, the uptake in MDA-MB-231 cells was clearly due to the folic acid as cells incubated with SA_1 were not significantly fluorescent.

Next, we evaluated the function of D (doxorubicin) and C (nucleus penetrating peptide) and their cooperativity in terms of the localization in the cells and cell toxicity. In particular, as doxorubicin stops DNA replication,[23] we aimed to deliver it into the cell nucleus using this peptide. We found that the trifunctional streptavidin conjugate $SA_1F_1D_1$ and tetrafunctional conjugate $SA_1F_1D_1C_1$ localized differently, when incubated with MDA-MB-231 cells (Fig. 4B). While $SA_1F_1D_1$ localized in the cytoplasm and was excluded from the nucleus, $SA_1F_1D_1C_1$ with the nucleus penetrating peptide localized in the nucleus, as observed with confocal microscopy. This finding was further supported through the quantification of the fluorescence signal within the nucleus of the cells (Fig. S13, ESI†). Moreover, both $SA_1F_1D_1$ and $SA_1F_1D_1C_1$ retained their selectivity for MDA-MB-231 cells over MCF-7 cells due to the folic acid modification (Fig. S11, ESI†).

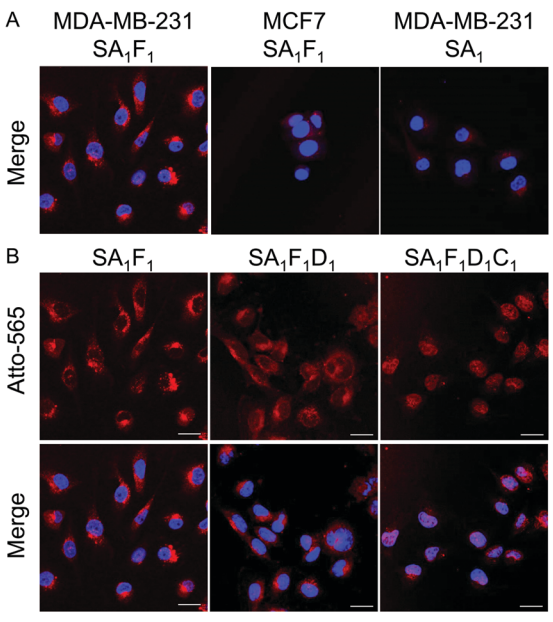

Fig. 4 (A) Confocal microscopy images of MDA-MB-231 (folate receptor positive) and MCF-7 (folate receptor negative) cells incubated with SA_1F_1 and MDA-MD-231 cells incubated with SA_1. (B) MDA-MB-231 cells were incubated with 1 μM SA_1F_1, $SA_1F_1D_1$ or $SA_1F_1D_1C_1$ in RPMI-1640 (no folic acid) medium for 4 hours. Atto-565 fluorescence shown in red and nuclei stained with DAPI are shown in blue. Scale bars are 25 μm. A: atto-565-biotin, F: folic acid–biotin, D: doxorubicin–biotin, C: nucleus penetrating peptide–biotin.

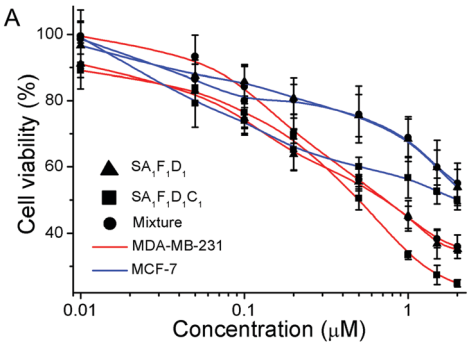

B

IC_{50} (μM)	MDA-MB-231	MCF-7
$SA_1F_1D_1$	0.74 ±0.12	2.62 ±0.78
$SA_1F_1D_1C_1$	0.50 ±0.08	2.00 ±0.80
Mixture	0.75 ±0.11	2.65 ±0.76

Fig. 5 (A) Cell viability of MDA-MB-231 and MCF-7 cells were incubated with $SA_1F_1D_1$, $SA_1F_1D_1C_1$ and a statistical mixture of streptavidin conjugates (S was mixed with one equivalent of A, F, D and C) for 72 hours. (B) Table of IC_{50} of different streptavidin conjugates. A: atto-565-biotin, F: folic acid–biotin, D: doxorubicin–biotin, C: nucleus penetrating peptide–biotin.

Next, we tested the cell toxicity of the multifunctional streptavidin conjugates in MDA-MB-231 and MCF-7 cells. The cell viability as measured using the MTT test after 72 h, showed that the tetrafunctional $SA_1F_1D_1C_1$ was the most effective drug against the aggressive MDA-MB-231 cells (Fig. 5). In $SA_1F_1D_1C_1$ and $SA_1F_1D_1$ the folic acid was responsible for the higher cell toxicity in MDA-MB-231 cells compared to MCF-7. While $SA_1F_1D_1C_1$ and $SA_1F_1D_1$ had IC_{50} of 0.5 μM and 0.74 μM for MDA-MB-231 cells, respectively, their IC_{50} for MCF-7 cells were higher at 2 μM and 2.62 μM, respectively. This amounts to a fourfold selectivity for MDA-MB-231 cells over MCF-7. For comparison, pure doxorubicin had no specificity and was almost equally cell toxic to both cell types (Fig. S14, ESI†). In $SA_1F_1D_1C_1$, the nucleus penetrating peptide, C, increased the delivery of doxorubicin, D, to the cell nucleus, which contributes to the higher final efficacy. As a result, $SA_1F_1D_1C_1$ had a lower IC_{50} of 0.5 μM compared to $SA_1F_1D_1$, which had a IC_{50} of 0.74 μM. The precise $SA_1F_1D_1$ conjugate also outperformed the statistical mixtures of conjugates (S mixed with one equivalent of A, F, D and C). In fact, the $SA_1F_1D_1C_1$ was 1.5 times more cell toxic than the statistical mixture of conjugates (IC_{50} 0.75 μM). Similarly, at 0.5 μM concentration MDA-MB-231 cells had a lower viability in the presence of $SA_1F_1D_1C_1$ (48%) than $SA_1F_1D_1$ (57%) or the statistical mixture (57%) (Fig. S15, ESI†). Moreover, the toxicity of all three conjugates decreased for MDA-MB-231 cells in the presence of excess folic acid, but not for MCF-7 cells, which confirmed the role of the folic acid for cell selectivity.

In summary, we demonstrated how stoichiometrically precise tetrafunctional streptavidin conjugates can be prepared to bring together multiple functionalities. In particular, we demonstrated how the delivery of an anti-cancer drug can be improved through the combination of a fluorescent, a cell targeting group, a nucleus penetrating peptide and a cell toxic drug in a tetrafunctional streptavidin. The systematic introduction of each functionality allows studying its effect on viability, targeting and efficacy, which improves our understanding on the essential features of drug delivery agents and enables optimization. The precise tetrafunctional streptavidins also open the door to assembly combinatorial libraries of exact streptavidins taking advantage of a wide repertoire of biotinylated molecules (proteins, peptides, small molecules, lipids and nucleic acids). Thus, our study plays a significant role in expanding the streptavidin–biotin chemistry in biotechnology, nanostructure assemblies and drug delivery.

This work is part of the MaxSynBio consortium, funded by the Federal Ministry of Education and Research (BMBF) of Germany (FKZ 031A359L) and the Max Planck Society. D. X. thanks the Chinese Scholarship Council for a PhD fellowship. T. W., S. L. K. and A. H. thank the Deutsche Forschungsgemeinschaft (DFG), 316249678-SFB 1279 (C01) for funding.

Open Access funding provided by the Max Planck Society.

Conflicts of interest

There are no conflicts to declare.

Notes and references

1 G. Destito, R. Yeh, C. S. Rae, M. G. Finn and M. Manchester, *Chem. Biol.*, 2007, **14**, 1152–1162.
2 F. M. F. Santos, J. N. Rosa, N. R. Candeias, C. P. Carvalho, A. I. Matos, A. E. Ventura, H. F. Florindo, L. C. Silva, U. Pischel and P. M. P. Gois, *Chem. – Eur. J.*, 2016, **22**, 1631–1637.
3 F. M. F. Santos, A. I. Matos, A. E. Ventura, J. Goncalves, L. F. Veiros, H. F. Florindo and P. M. P. Gois, *Angew. Chem., Int. Ed.*, 2017, **56**, 9346–9350.
4 O. Boutureira and G. J. L. Bernardes, *Chem. Rev.*, 2015, **115**, 2174–2195.
5 A. Maruani, M. E. B. Smith, E. Miranda, K. A. Chester, V. Chudasama and S. Caddick, *Nat. Commun.*, 2015, **6**, 6645.
6 Y. Y. Kim, Y. Bang, A. H. Lee and Y. K. Song, *ACS Nano*, 2019, **13**, 1183–1194.
7 M. Piffoux, A. K. A. Silva, C. Wilhelm, F. Gazeau and D. Tareste, *ACS Nano*, 2018, **12**, 6830–6842.
8 M. Srinivasarao and P. S. Low, *Chem. Rev.*, 2017, **117**, 12133–12164.
9 N. Habibi, N. Kamaly, A. Memic and H. Shafiee, *Nano Today*, 2016, **11**, 41–60.
10 S. Scarabelli, K. T. Tan, R. Griss, R. Hovius, P. L. D'Alessandro, T. Vorherr and K. Johnsson, *ACS Sens.*, 2017, **2**, 1191–1197.
11 L. Xue, Q. Yu, R. Griss, A. Schena and K. Johnsson, *Angew. Chem., Int. Ed.*, 2017, **56**, 7112–7116.
12 R. Pasqualini and E. Ruoslahti, *Nature*, 1996, **380**, 364–366.
13 N. M. Green, *Methods Enzymol.*, 1990, **184**, 51–67.
14 M. Howarth, D. J. F. Chinnapen, K. Gerrow, P. C. Dorrestein, M. R. Grandy, N. L. Kelleher, A. El-Husseini and A. Y. Ting, *Nat. Methods*, 2006, **3**, 267–273.
15 G. V. Dubacheva, C. Araya-Callis, A. G. Volbeda, M. Fairhead, J. Codee, M. Howarth and R. P. Richter, *J. Am. Chem. Soc.*, 2017, **139**, 4157–4167.
16 D. Kalderon, B. L. Roberts, W. D. Richardson and A. E. Smith, *Cell*, 1984, **39**, 499–509.
17 V. Gaberc-Porekar and V. Menart, *Chem. Eng. Technol.*, 2005, **28**, 1306–1314.
18 S. L. Kuan, D. Y. W. Ng, Y. Z. Wu, C. Fortsch, H. Barth, M. Doroshenko, K. Koynov, C. Meier and T. Weil, *J. Am. Chem. Soc.*, 2013, **135**, 17254–17257.
19 D. Xu and S. V. Wegner, *Chem. Sci.*, 2020, **11**, 4422–4429.
20 R. Mittal and M. P. Bruchez, *Bioconjugate Chem.*, 2011, **22**, 362–368.
21 Y. Ma, M. Sadoqi and J. Shao, *Int. J. Pharm.*, 2012, **436**, 25–31.
22 A. Eguchi, H. Furusawa, A. Yamamoto, T. Akuta, M. Hasegawa, Y. Okahata and M. Nakanishi, *J. Controlled Release*, 2005, **104**, 507–519.
23 Y. Pommier, E. Leo, H. L. Zhang and C. Marchand, *Chem. Biol.*, 2010, **17**, 421–433.